Available online at www.sciencedirect.com
SCIENCE DIRECT®
Organic Electronics 4 (2003) 61–69
Organic Electronics
www.elsevier.com/locate/orgel

Highly efficient light emitters based on the spiro concept

Till Spehr, Robert Pudzich, Thomas Fuhrmann, Josef Salbeck *

Macromolecular Chemistry and Molecular Materials, Department of Science and Center for Interdisciplinary Nanostructure Science and Technology (CINSaT), University of Kassel, Heinrich-Plett-Str. 40, D-34109 Kassel, Germany

Abstract

We present a comparison of different molecular glasses based on the spiro-concept with respect to their photoemission properties. The absorption and emission spectra as well as the photoluminescence quantum yields in solution are characterized. For thin amorphous films, prepared by vacuum vapor deposition, we examined amplified spontaneous emission (ASE) by optical pumping with picosecond pulses at 337 nm. Efficient ASE emission with thresholds of down to 1 $\mu J/cm^2$ was observed.

PACS: 78.20.Ci; 78.45.+h; 78.55.Kz; 78.66.Qn; 33.50.Dq
Keywords: Organic laser; Stimulated emission; Amplified spontaneous emission; Spiro compounds; Oligophenyl; Carbazole

1. Introduction

Spiro-type molecular glasses are promising candidates for solid-state lasing since they combine excellent emitting properties of the incorporated chromophores with a high morphological stability of the glassy state. The common structural feature of spiro compounds is the linkage of two aromatic chromophores by an additional carbon atom (spiro-junction). The rigid structure of the star-shaped molecules leads to a molecular entanglement in the solid state and prevents crystallization. Almost all materials based on this concept can be prepared in the amorphous glassy state, with glass transition temperatures well above room temperature [1].

Since the chromophores are arranged perpendicularly, only a weak interaction between the molecular halves is expected, which means that the electronic character of the individual chromophores is preserved [2]. Whether a chromophore is suitable in an appropriate spiro version as a laser dye in solid films depends on the intrinsic fluorescence properties of the molecules as well as on the intermolecular interactions in the solid state which may also result in excitation quenching and excimer formation.

A good test of the ability for stimulated emission processes in undiluted films are amplified spontaneous emission (ASE) experiments, in which the compound is optically pumped in a thin film waveguide geometry. Stimulated emission can be seen as narrowing of the emission spectrum to a line when the pump intensity exceeds a certain threshold value. Spiro-oligophenyls such as Spiro-sexiphenyl **1** and branched spiro compounds of higher generations like 4-Spiro [2] **2** have been

* Corresponding author. Tel.: +49-561-804-4425; fax: +44-561-804-4555.
E-mail address: salbeck@uni-kassel.de (J. Salbeck).

1566-1199/$ - see front matter © 2003 Elsevier B.V. All rights reserved.
doi:10.1016/j.orgel.2003.08.002

proven as efficient blue emitters in spin-coated or vacuum deposited amorphous films [3,4]. They show ASE behaviour with threshold intensities as low as 3.2 μJ/cm^2 and ASE linewidths of about 2–3 nm.

In this contribution, we extend the range of spiro compounds which have been investigated with regard to their emission behaviour. We will give an overview about the photoluminescence and stimulated emission behaviour of different functional classes of spiro compounds. The chemical structures of the materials treated in this report are shown in Figs. 1 and 2, the thermodynamical data are summarized in Table 1.

Spiro-6ϕ(MeO)$_4$ **3** and Spiro-Octo2 **4** can be considered as structural derivatives of Spiro-sexiphenyl by additional substitution with four methoxy groups or two biphenyl groups, respectively. Spiro-DPVBi **5** is the spiro variant of the blue emitting dye DPVBi and has been used as an efficient and morphologically stable substitute for DPVBi in organic light emitting diodes [5].

In organic light emitting diodes and other electrically driven devices, good emitters should also exhibit some charge transporting properties, so we investigated the following compounds: Spiro-PBD **6** is based on the oxadiazole moiety known as violet emitting chromophore in dye lasers and as an electron transporting compound in organic light emitting diodes [6]. In Spiro-SPO **7**, the spiro-junction combines two different chromophores: a sexiphenyl chain and an oxadiazole moiety. The concept behind the design of this molecule is to separate charge transport and luminescence properties retaining the homogeneous character of solid films. Spiro-TAD **8** is a hole transporting material. The emission properties of glass forming aryl amines like **8** become more interesting since ASE was detected for its parent compound, TPD [7]. Spiro-Carb **9** is the corresponding carbazole compound. Carbazoles have been used as photoconductors and are interesting as host materials for phosphorescent emitters. For example, 4–4′-*N*–*N*′-Dicarbazole-biphenyl (CBP) was applied as matrix in electrophosphorescent devices containing platinum and iridium complexes [8], and it can be expected that Spiro-Carb may be a good replacement for CBP due to its high morphological stability (glass transition temperature 240 °C, melting point 538 °C). Finally, the compounds Spiro-AMO-*t*Bu **10** and Spiro-AMPO-*t*Bu **11** are bipolar, combining a triphenylamine and an oxadiazole moiety in a donor-acceptor type conjugated π-electron system. All materials form stable amorphous films and are thus suitable for waveguide applications. The glass transition temperatures are summarized in Table 1, they cover a range from 130 to 273 °C.

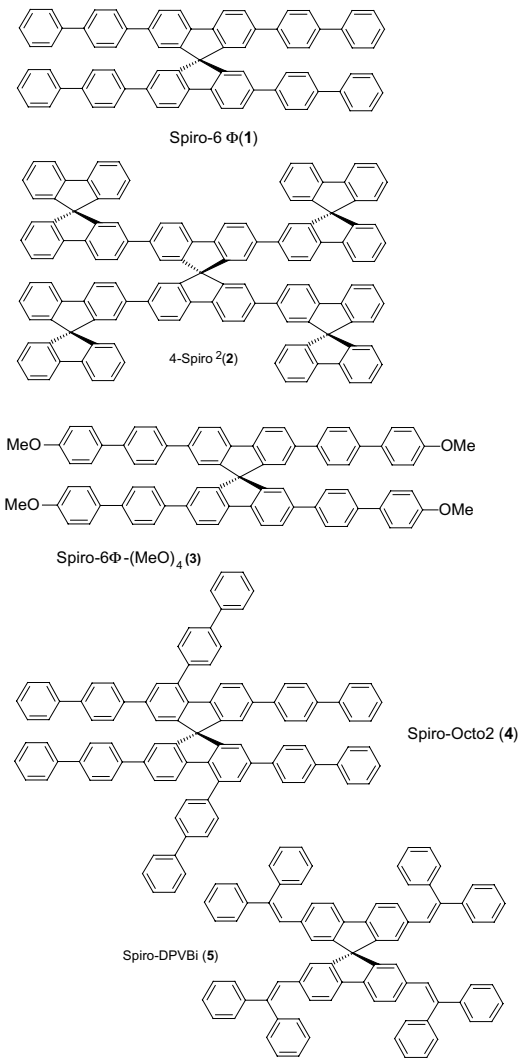

Fig. 1. Chemical structures of the investigated oligophenyl emitter materials.

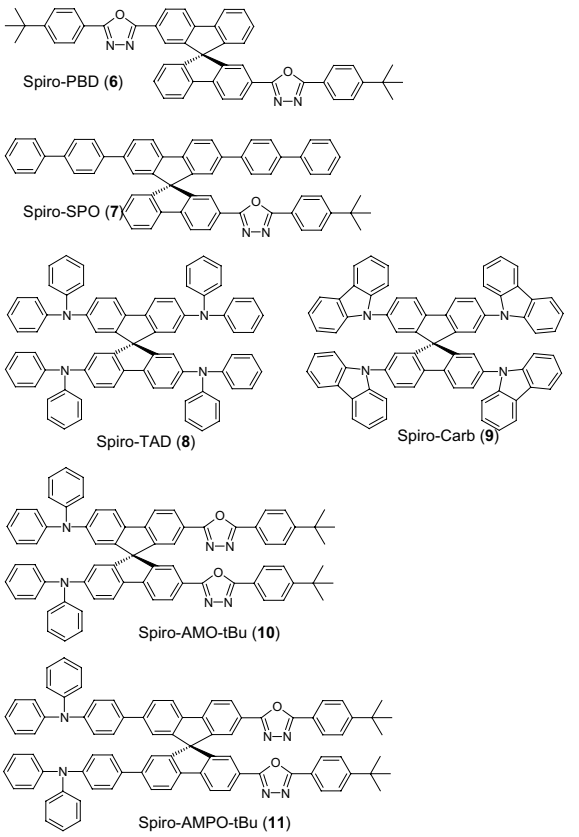

Fig. 2. Chemical structures of the bifunctional charge transporting/emitting materials.

Table 1
Thermodynamic data of the investigated compounds, obtained by differential scanning calorimetry (T_g glass transition temperature, T_m melting point)

Compound	T_g [°C]	T_m [°C]
Spiro-6ϕ (**1**)	212	408
4-Spiro^2 (**2**)	273	447
Spiro-6ϕ(MeO)$_4$ (**3**)	191	326
Spiro-Octopus (**4**)	236	263
Spiro-DPVBi (**5**)	130	228
Spiro-PBD (**6**)	163	337
Spiro-SPO (**7**)	177	
Spiro-TAD (**8**)	133	275
Spiro-Carb (**9**)	240	538
Spiro-AMO-*t*Bu (**10**)	165	
Spiro-AMPO-*t*Bu (**11**)	177	

Compounds for which no melting point is given, have been obtained only in the amorphous state.

2. Experimental

The synthesis of the spiro compounds is described elsewhere [9,10]. Spiro-DPVBi was obtained from Covion Organic Semiconductors, Germany.

Thermal transition temperatures were determined by DSC on a Perkin-Elmer DSC-7 Thermal Analyser under a continuous N_2 flow of 15 ml/min. Samples were first heated to beyond crystalline melting points followed by cooling at −20 to −30 °C/min before taking the second heating scans at 10 °C/min.

Absorption spectra were recorded with a Perkin Elmer lambda900 spectrophotometer. Fluorescence spectra, excitation spectra and quantum yields were measured with a Hitachi f-4500 fluorescence spectrophotometer.

Quantum yields were determined in degassed solutions with an optical density of approximately 0.02. Spiro-6ϕ was referenced against recrystallized quinine sulfate dihydrate in 0.05 mol/l H_2SO_4 with a standard reference quantum yield of 57.7% [11]. Calibration due to detector response and solvent scattering as well as refractive index correction for the solvent was applied [12]. All other compounds were referenced against Spiro-6ϕ using the same solvent. Spectroscopic grade solvents (Merck UVASOL) were used without further purification.

Thin films were prepared by vacuum vapor deposition at a pressure of 1×10^{-6} mbar and a rate of 0.05 nm/s from quartz crucibles in an evaporation system from Bestec GmbH, Germany. Thermally oxidized Si wafers were used as substrates, with oxide thicknesses of 1.8–2.1 μm.

Film thicknesses and refractive indices were measured by variable angle spectroscopic ellipsometry with a Woollam VASE ellipsometer. Isotropic Cauchy modelling [13] was used, fitting from 1000 nm down to the wavelength of the emission maximum. The latter is usually still well separated from the region of absorption, justifying the Cauchy assumption for the dispersion behaviour.

ASE experiments were performed in a self-constructed chamber with quartz windows and controllable inert gas atmosphere (see Fig. 3). For

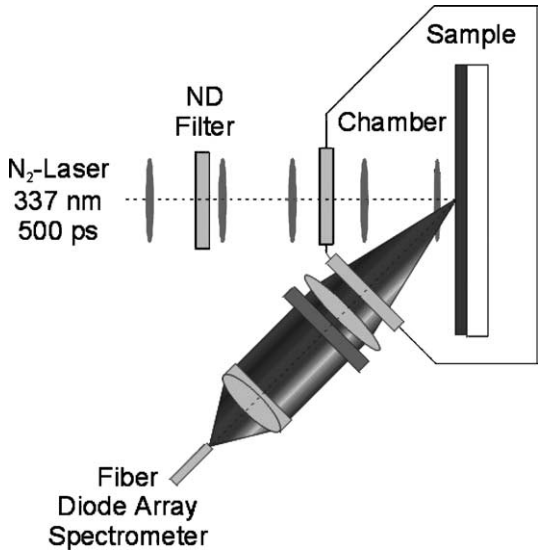

Fig. 3. Setup for amplified spontaneous emission (ASE) experiments. The sample is placed in a nitrogen-filled chamber and is irradiated with a pulsed nitrogen laser at 337 nm. The scattered ASE light is collected and coupled into a diode array spectrometer for spectral analysis.

the excitation, a nitrogen laser (Lasertechnik Berlin MSG 800) at 337 nm (500 ps pulses, 10 Hz) was used. The maximum intensity at the position of the sample was 336 μJ/cm^2, as measured with a LTB pyroelectric detector. The excitation intensity was varied by a neutral density filter wheel. The samples were irradiated under normal incidence. The scattered luminescence light was collected at an angle of 60° with a lens ($f = 30$ mm) and focused with a microscope objective (10×) to a 200 μm optical fiber (NA 0.22). The fiber was connected to a calibrated Ocean Optics S 2000 fiber spectrometer for spectra acquisition (integration time 1 s, averaged over 60 spectra, 1 nm resolution).

3. Results and discussion

3.1. Photoluminescence properties and quantum yields in solution

The absorption and emission data of the compounds in solution are given in Table 2. Generally, the spectroscopic behaviour of the materials is characterized by a large Stokes shift between the absorption and emission maxima in the order of 30–70 nm. Vibronic splitting in several side maxima can be observed, especially for the oligophenyl and oxadiazole compounds. The mixed compound Spiro-SPO (**7**) shows the characteristic emission behaviour of its sexiphenyl component whereas the absorption spectra can be regarded as a summation of both chromophores, as can be seen when its spectrum is compared with the spectra of **1** and **6**.

The absorption maxima differ only slightly in solvents of different polarity, whereas solvatochromic effects due to a different stabilization of the excited state can be seen in the fluorescence spectra. For Spiro-TAD (**8**) and Spiro-Carb (**9**), a stabilization energy of 60–80 meV is obtained by changing the solvent from cyclohexane to dichloromethane. For the bipolar compounds Spiro-AMO-*t*Bu (**10**) and Spiro-AMPO-*t*Bu (**11**), the bathochromic shift is much more pronounced, with energy differences of 420 and 480 meV, respectively. In contrast, the non-polar oligophenyles and the oxadiazoles show only negligible shift.

The quantum yields have been determined in cyclohexane for comparison. The emitting material with the highest quantum yield of 98% is Spiro-6ϕ (**1**), followed by the branched oligophenyles 4-Spiro^2 (**2**) and Spiro-Octo2 (**4**) with 96% and 95%, respectively. Spiro-6ϕ(MeO)$_4$ (**3**), Spiro-DPVBi (**5**), Spiro-PBD (**6**) and the mixed compound Spiro-SPO (**7**) show reasonable values between 75 and 87%. The quantum yield of Spiro-Carb (**9**) lies with 83% in the same range. This for an amino compound rather high value is attributed to the rigidity of the carbazole group. Spiro-TAD (**8**) and the bipolar compounds **10** and **11** have a lower efficiency being higher in a stabilizing polar environment than in a non-polar solution.

3.2. Amplified spontaneous emission in thin films

All materials can be prepared as amorphous thin films by vacuum vapor deposition. As it is known that stimulated emission with the lowest threshold is obtained for optical monomode films just above the cutoff thickness [4,14], the film thicknesses have been chosen accordingly between

Table 2
Spectra and quantum yields in solution (λ_{max} absorption maxima, λ_{em} fluorescence maxima, Qu.y. fluorescence quantum yield)

	λ_{max} [nm] (CH_2Cl_2)	λ_{em} [nm] (CH_2Cl_2)	λ_{max} [nm] (C_6H_{12})	λ_{em} [nm] (C_6H_{12})	Qu.y. (C_6H_{12})
Spiro-6ϕ (**1**)	343	386 (405)	340	381	0.98
4-Spiro^2 (**2**)	353	396 (418)	350	393 (413)	0.96
Spiro-6ϕ(MeO)$_4$ (**3**)	353	392 (412)	343	387 (405)	0.87
Spiro-Octo2 (**4**)	345	397 (412)	343	396	0.95
Spiro-DPVBi (**5**)	377	453	375	452	0.82
Spiro-PBD (**6**)	330	373 (355, 393)	328	370 (351, 386)	0.75
Spiro-SPO (**7**)	331	386 (405)	345	381 (399)	0.87
Spiro-TAD (**8**)	378	402	379	394 (413)	0.42
Spiro-CARB (**9**)	340	372	347	363 (380)	0.83
Spiro-AMO-*t*Bu (**10**)	389	477	397	411 (434)	0.56
Spiro-AMPO-*t*Bu (**11**)	374	497	374	416 (441)	0.58

Values in parentheses denote minor, but clearly visible maxima. Quantum yields are given within ±5%.

50 and 130 nm, but they were not optimized for the individual compounds. The emission spectra of the films resemble the solution spectra, with a shift of the emission maximum which is determined by the relative polarity of the compounds in the solid state. As an example, the solution and film spectra of Spiro-SPO (**7**) are shown in Fig. 4. The film emission spectrum is approximately 20 nm bathochromically shifted with respect to dichloromethane solution, and the second vibronic band has gained a higher intensity. For comparison, the spectrum of a spincoated film is shown as well. Here, the relative intensities of the first and second vibronic band are almost equal. For the bipolar compounds **10** and **11**, the fluorescence maxima in the solid state are close to the spectra in CH_2Cl_2, indicating a similar polarity of the environment. For Spiro-TAD (**8**), a broad emission around 460–480 nm was detected in the solid state which is not found in solution and can be attributed to excimer formation due to intermolecular interactions. A similar observation, but less distinct, was made for Spiro-PBD (**6**). Table 3 displays the optical data in the solid state.

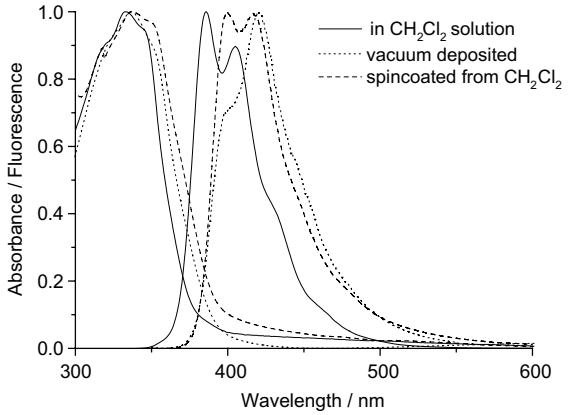

Fig. 4. Absorption and emission spectra of Spiro-SPO (**7**) in CH_2Cl_2 solution and in vacuum deposited and spincoated thin films. The solid state spectra are bathochromically shifted, and the relative intensities of the maxima depend on the preparation conditions. The emission spectrum in cyclohexane (not shown) is similar to the spectrum in CH_2Cl_2, but 5 nm blueshifted.

By excitation of the films with pulses at 337 nm, line narrowing was investigated for the different materials. Fig. 5 shows an example for the observed change in the emission spectra of the compound Spiro-SPO (**7**). At low irradiation intensities, the normal photoluminescence spectrum is observed. At intensities in excess of several μJ/cm^2, the spectrum changes and emission intensity is gained in the peak at 419 nm at the cost of other vibronic bands, resulting in a narrow ASE line. The ASE line corresponds to the fluorescence maximum in most but not in all cases. For Spiro-DPVBi (**5**), the film fluorescence maximum is at 466 nm, the ASE line at 475 nm. For Spiro-PBD (**6**), the most intense fluorescence band is the second vibronic band at 406 nm, whereas the amplified mode is the first vibronic band at 387 nm. A similar behaviour has been observed previously in the case of Spiro-quaterphenyl [3]. In contrast, for

Table 3
Optical data of the films prepared by vapor deposition (α attenuation coefficient at pump wavelength and absorption maximum, respectively, λ_{max} absorption maxima, λ_{em} fluorescence maxima)

	α [10^{-2} nm^{-1}] (337 nm)	α [10^{-2} nm^{-1}] (λ_{max})	λ_{max} [nm] Film	λ_{em} [nm] Film
Spiro-6ϕ(MeO)$_4$ (**3**)	3.08	3.32	349	430
Spiro-Octo2 (**4**)	1.45	1.56	350	433
Spiro-DPVBi (**5**)	0.76	0.86	359	466
Spiro-PBD (**6**)	1.88	1.94	334	406
Spiro-SPO (**7**)	3.03	3.03	337	420
Spiro-TAD (**8**)	1.10	1.88	383	406
Spiro-CARB (**9**)	1.90	2.30	346	382
Spiro-AMO-*t*Bu (**10**)	0.90	1.70	389	472
Spiro-AMPO-*t*Bu (**11**)	1.09	1.36	376	479

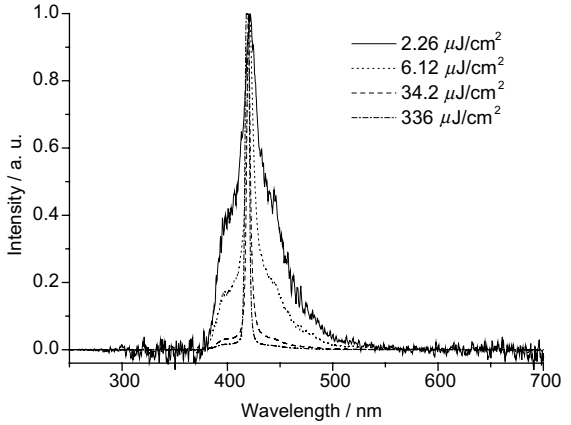

Fig. 5. Line narrowing by stimulated emission in a thin film of Spiro-SPO (**7**) above threshold. With increasing pump intensity, the ASE line becomes smaller, and vibronic side bands are suppressed.

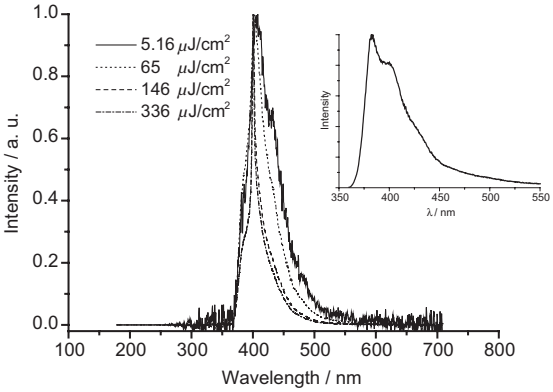

Fig. 6. Line narrowing by stimulated emission in a thin film of Spiro-Carb (**9**). The inset shows the normal fluorescence spectrum of an vacuum deposited film. Here, the ASE line corresponds to a higher vibrational mode. Note that on the short-wavelength side, the ASE spectrum is cut off because of a 380 nm edge filter in the detection beam path.

Spiro-Carb (**9**) it is the second vibronic band that is amplified (Fig. 6), and the first one exhibits the maximum in the normal fluorescence. These differences can be attributed to an interplay between stimulated gain and absorption losses, the latter one being larger at small wavelengths.

The materials can be roughly divided into three groups according to their ASE behaviour. For the first group, showing the best ASE behaviour, the transition of line narrowing can easily be detected in the pump intensity range up to 350 μJ/cm^2. In addition to the compounds Spiro-6ϕ (**1**) and Spiro^2 (**2**), which are discussed more in detail in a previous publication [4], the compounds Spiro-Octo2 (**4**), Spiro-SPO (**7**), and, less markedly, Spiro-Carb (**9**) and Spiro-6ϕ(MeO)$_4$ (**3**) belong to this group. For the second group, the onset of ASE peak formation can be detected by using additional focusing with a cylindrical lens, leading to pump intensities of several mJ/cm^2. This group comprises Spiro-DPVBi (**5**), Spiro-TAD (**8**) and Spiro-PBD (**6**). Finally, for Spiro-AMO-*t*Bu (**10**) and Spiro-AMPO-*t*Bu (**11**) no amplified spontaneous emission could be detected under the present excitation conditions.

For the first group, peak widths (full width at half maximum, FWHM) of the peaks at an irra-

diation intensity of 336 μJ/cm^2 and threshold intensities have been determined according to the procedure described in [4]. The plot of FWHM versus the pulse energy (on a logarithmic scale) gives a sigmoidal curve which is fitted with the function

$$\mathrm{FWHM}(x) = \frac{A1 - A2}{1 + (x/x_0)^p} + A2,$$

in which x means pulse energy, $A1$ and $A2$ the FWHM in the low and high pulse energy limit, respectively. x_0 is the pulse energy for FWHM $= (A1 + A2)/2$, and p represents the steepness of the function. The intersection of the tangent at the turning point and the normal fluorescence linewidth (FWHM $= A1$) defines the threshold intensity. As an example, the dependence of FWHM on pump intensity is displayed in Fig. 7 for Spiro-SPO (**7**). For this compound, the lowest threshold with 1 μJ/cm^2 was obtained, followed by Spiro-Octo2 (**4**) with 3 μJ/cm^2. These values are even lower than the values determined for Spiro-6ϕ (**1**) and 4-Spiro^2 (**2**) with 3.2 and 11 μJ/cm^2, respectively [4]. The linewidths are of the same order of magnitude but slightly larger than measured for Spiro-6ϕ (2.9 nm) and 4-Spiro^2 (3.2 nm) [4].

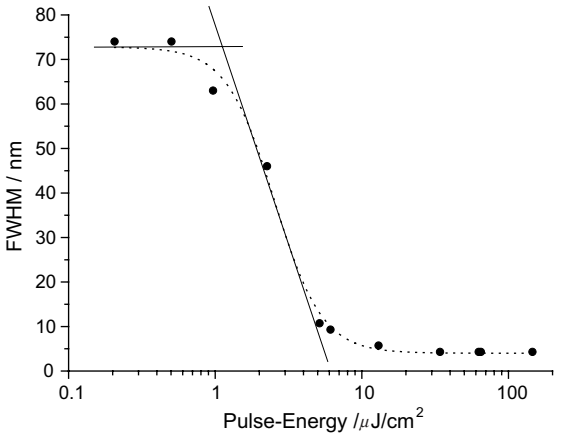

Fig. 7. Full width at half maximum versus pump intensity for Spiro-SPO (**7**). The dotted line corresponds to a sigmoidal fit curve to the data. The intersection of the tangent to the turning point and the fluorescence linewidth defines the threshold intensity.

The ASE behaviour of the compounds is summarized in Table 4. For a direct comparison one should note that the optical efficiency of pumping a certain waveguide mode is influenced by the film thickness and the effective index of the mode and is not yet optimized for the individual compounds. In all cases, it can be assumed that the amplified waveguide mode is the TE_0 mode with a transversal electric field polarization corresponding to the excitation polarization. We confirmed this by a polarization analysis of the ASE light, which shows predominantly TE polarization. The effective index n_{eff} and electric field distribution $E(z)$ of the TE_0 mode can be calculated easily by standard methods [15]. The relative coupling of an excited dipole to this mode depends on the local field intensity whereas the excitation probability of the dipole in a layer dz is governed by the penetration depth of the exciting light. Modifying the formula given in Ref. [4], we calculate the relative excitation efficiency factor as

$$f = \frac{\eta_{\mathrm{eff}}}{2c\mu_0} \int_0^d \alpha_{337} \exp(-\alpha_{337} z) E^2(z)\, \mathrm{d}z,$$

where n_{eff} is the effective mode index; c the vacuum speed of light; μ_0 the vacuum permeability; α the attenuation coefficient of pump light; d is the film thickness. Here, the field profiles of the ASE modes are normalized by a power flow of 1 W per unit width [15]. The Fresnel transmission coefficients at the film surface are neglected in this approximation since the refractive indices at the excitation wavelength can be regarded as similar for all materials (surface transmission 80–90%), giving only a minor influence. Mainly due to differences in the absorption coefficient and therefore in the amount of absorbed light, the relative excitation factors differ by a factor of 3 for the investigated samples, as can be seen in Table 4. This value cannot explain the large differences between the ASE threshold values of the distinct groups of materials, clearly distinguishing materials with high and moderate ASE efficiency. The difference between these groups has to be attributed to the different photophysical behaviour, especially the quantum yields. Indeed, there is a rough correlation between quantum yields in solution and ASE

Table 4
Results of ASE experiments with the films from Table 3

	d [nm]	λ_{ASE} nm	FWHM [nm]	J_{TH} μJ/cm^2	n (λ_{ASE})	n_{eff} TE_0	f [10^9 W/m^2]
Spiro-6ϕ(MeO)$_4$ (**3**)	50	427.5	9.3	30	2.15	1.58	2.83
Spiro-Octo2 (**4**)	66	425.4	4.6	3	1.80	1.48	1.00
Spiro-DPVBi (**5**)	61	475.3	n.d		1.94	1.51	0.86
Spiro-PBD (**6**)	70	386.7	n.d		1.86	1.54	1.99
Spiro-SPO (**7**)	122	419.0	5.4	1	1.98	1.73	2.25
Spiro-TAD (**8**)	98	404.7	n.d		2.04	1.74	2.07
Spiro-CARB (**9**)	117	400.3	7.9	50	2.11	1.86	2.34
Spiro-AMO-*t*Bu (**10**)	126	–			1.88	1.63	1.65
Spiro-AMPO-*t*Bu (**11**)	111	–			1.85	1.58	1.74

d Film thickness, λ_{ASE} peak wavelength, FWHM full width at half maximum, J_{TH} threshold intensity, n refractive index, n_{eff} calculated effective index for TE_0 waveguide mode, f excitation efficiency factor for TE_0 mode, as defined in the text.

performance. For a quantitative evaluation, however, the quantum yields in the solid state have to be compared. The complete data are not yet available, but experimental work for the determination of the values is in progress. For an individual material with a given quantum yield in the bulk, the efficiency can be further improved by optimizing the film thickness. The dependence of the quantum yield on film thickness is assumed to be small, the major effect being the influence of the excitation penetration depth and the field profile of the amplified mode. Low thresholds as for example measured for the Spiro-SPO device are attributed to a favorable combination of high quantum yields, high absorbance and optimized waveguide design. For all materials, further improvement by optimizing the film parameters in order to obtain devices with lower thresholds should be possible. These issues are currently under investigation.

4. Conclusion

Among the new spiro compounds investigated for stimulated emission in thin films, the combined electron transport/emitting material Spiro-SPO and other substituted oligophenyl compounds like Spiro-Octo2 proved to be very efficient with low ASE thresholds. Also the carbazole Spiro-Carb exhibits remarkable ASE behaviour. The respective performance in ASE experiments roughly correlates with the fluorescence quantum yields measured in cyclohexane solution. Due to their optical properties and morphological stability, the materials are promising candidates for solid state light sources.

Acknowledgements

We thank Lothar Weissenborn for his assistance in sample preparation and characterization, Frank Weissörtel, Andrea Lux and Andreas Kettner for materials synthesis, and Rainer Bausch for discussion. We thank the Institute for Microstructure Technology and Analytics, University of Kassel, for granting us access to their equipment for thermal oxidation of Si-wafers. Support by Covion Organic Semiconductors and financial support by the University of Kassel (ZFF) is gratefully acknowledged.

References

[1] J. Salbeck, N. Yu, J. Bauer, F. Weissörtel, H. Bestgen, Synth. Met. 91 (1997) 209.
[2] N. Johansson, D.A. dos Santos, S. Guo, J. Cornil, M. Fahlman, J. Salbeck, H. Schenk, H. Arwin, J.L. Bredas, W.R. Salaneck, J. Chem. Phys. 107 (1997) 2542.
[3] N. Johansson, J. Salbeck, J. Bauer, F. Weissoertel, P. Broems, A. Andersson, W.R. Salaneck, Adv. Mater. 10 (1998) 1136.
[4] J. Salbeck, M. Schörner, T. Fuhrmann, Thin Solid Films 417 (2002) 20.
[5] H. Spreitzer, H. Schenk, J. Salbeck, F. Weissörtel, H. Riel, W. Riess, Proc. SPIE 3797 (1999) 316.
[6] C. Adachi, T. Tsutsui, S. Saito, Appl. Phys. Lett. 55 (1989) 1489.

[7] W. Holzer, A. Penzkofer, H. Hörhold, Synth. Met. 113 (2000) 281.
[8] M.A. Baldo, S. Lamansky, P.E. Burrows, M.E. Thompson, S.R. Forrest, Appl. Phys. Lett. 75 (1999) 4.
[9] F. Weissörtel, Ph.D. Thesis, University of Regensburg, Regensburg, Germany, 1999.
[10] R. Pudzich, Ph.D. thesis, University of Kassel, Kassel, Germany, 2003.
[11] N. DiCesare, J.R. Lakowicz, J. Phys. Chem. A 105 (2001) 6834.
[12] J.V. Morris, M.A. Mahaney, J.R. Huber, J. Phys. Chem. 80 (1976) 969.
[13] H.G. Tompkins, W.A. McGahan, Spectroscopic Ellipsometry and Reflectrometry, John Wiley & Sons, New York, 1999.
[14] T.W. Lee, O.O. Park, D.H. Choi, H.N. Cho, Y.C. Kim, Appl. Phys. Lett. 81 (2002) 424.
[15] P. Yeh, Optical Waves in Layered Media, John Wiley & Sons, New York, 1988.